CHEMISTRY OF MATERIALS
Article

Chem. Mater. **2010,** *22,* 5707–5711 5707
DOI:10.1021/cm101724t

Applications of Tunable TiO_2 Nanotubes as Nanotemplate and Photovoltaic Device

Dongdong Li,[†,‡] Pai-Chun Chang,[‡] Chung-Jen Chien,[‡] and Jia G. Lu*[,‡]

[†]*Division of Energy and Environmental Research, Shanghai Advanced Research Institute, Chinese Academy of Sciences, Shanghai 201203, People's Republic of China, and* [‡]*Departments of Physics & Electrophysics, University of Southern California, Los Angeles, California 90089-0484, United States*

Received June 20, 2010. Revised Manuscript Received August 12, 2010

Highly ordered anodic titanium oxide (ATO) TiO_2 nanotube film has been synthesized via a typical two-step anodization method. Following a reductive doping approach, metallic materials (copper and nickel) can be efficiently electrodeposited into the nanotubes. This versatile process yields reproducible tubular structures in ATO membranes, because of the conductive nature of crystallized TiO_2, yielding promising potential for nanotemplate applications. In this paper, we present a dye-sensitized solar cell constructed by employing such ATO films. It is observed that the reductive doping treatment can also enhance the solar cell's short current density and fill factor, resulting in an improved energy conversion efficiency.

1. Introduction

Titanium oxide (TiO_2) is an *n*-type semiconductor with a bandgap energy of 3.0−3.2 eV. It has broad applications, because of the versatile functionalities.[1−3] Synthesis of anodic titanium oxide (ATO) nanotube templates has gained significant progress in fluoride-ion-contained electrolytes.[4] The one-dimensional (1D) structure provides a large specific surface area as well as a direct pathway for charge transport, thus rendering superior capabilities in light-harvesting,[5,6] electrochromic switching,[7] environmental sensing,[8−10] energy storage,[11−13] etc. The construction of three-dimensional (3D) core−shell structures by employing TiO_2 nanotube templates has been demonstrated on various guest materials via electrodeposition.[13−17] The ordered heterojunction provides an ideal system for energy harvesting and storage devices. However, high-efficiency filling of the entire pore network remains a challenge, because of the small pore size and conformably conductive nature of the host material. To overcome this problem, Grimes and co-workers have developed a rational dipping and deposition method where CdTe/TiO_2 photoelectrodes can be realized.[18] Nevertheless, many cycles are required in forming high-quality conformal junctions. It is worth noting that Schmuki and co-workers have developed a reductive doping process to form a more conductive layer at the nanotube bottom.[19,20] Motivated by the in situ doping method, we have successfully filled *p*-type Cu_2O into *n*-type TiO_2 nanotubes and created *p*−*n* heterojunctions along the radial direction in the three-dimensional (3D) matrix.[21] The 3D core−shell *p*−*n* junction arrays show improved photovoltaic (PV) performance, because of the greatly increased interface area, and efficient charge separation and transport process.

*Author to whom correspondence should be addressed. E-mail: jia.grace.lu@usc.edu.

(1) Nazeeruddin, M. K.; Pechy, P.; Renouard, T.; Zakeeruddin, S. M.; Humphry-Baker, R.; Comte, P.; Liska, P.; Cevey, L.; Costa, E.; Shklover, V.; Spiccia, L.; Deacon, G. B.; Bignozzi, C. A.; Grätzel, M. *J. Am. Chem. Soc.* **2001**, *123*, 1613.
(2) Chiba, Y.; Islam, A.; Watanabe, Y.; Komiya, R.; Koide, N.; Han, L. Y. *Jpn. J. Appl. Phys., Part 2* **2006**, *45*, L638.
(3) Asahi, R.; Morikawa, T.; Ohwaki, T.; Aoki, K.; Taga, Y. *Science* **2001**, *293*, 269.
(4) Paulose, M.; Shankar, K.; Yoriya, S.; Prakasam, H. E.; Varghese, O. K.; Mor, G. K.; Latempa, T. A.; Fitzgerald, A.; Grimes, C. A. *J. Phys. Chem. B* **2006**, *110*, 16179.
(5) Varghese, O. K.; Paulose, M.; Grimes, C. A. *Nat. Nanotechnol.* **2009**, *4*, 592.
(6) Shankar, K.; Basham, J. I.; Allam, N. K.; Varghese, O. K.; Mor, G. K.; Feng, X. J.; Paulose, M.; Seabold, J. A.; Choi, K. S.; Grimes, C. A. *J. Phys. Chem. C* **2009**, *113*, 6327.
(7) Ghicov, A.; Alba, S. P.; Macak, J. M.; Schmuki, P. *Small* **2008**, *4*, 1063.
(8) Varghese, O. K.; Gong, D. W.; Paulose, M.; Ong, K. G.; Grimes, C. A. *Sens. Actuators B* **2003**, *93*, 338.
(9) Varghese, O. K.; Grimes, C. A. *J. Nanosci. Nanotechnol.* **2003**, *3*, 277.
(10) Rani, S.; Roy, S. C.; Paulose, M.; Varghese, O. K.; Mor, G. K.; Kim, S.; Yoriya, S.; LaTempa, T. J.; Grimes, C. A. *Phys. Chem. Chem. Phys.* **2010**, *12*, 2780.
(11) Fang, D.; Huang, K. L.; Liu, S. Q.; Li, Z. J. *J. Alloys Compd.* **2008**, *464*, L5.
(12) Kim, M. S.; Lee, T. W.; Parka, J. H. *J. Electrochem. Soc.* **2009**, *156*, A584.
(13) Xie, Y.; Zhou, L.; Huang, C.; Huang, H.; Lu, J. *Electrochim. Acta* **2008**, *53*, 3643.
(14) Banerjee, S.; Mohapatra, S. K.; Das, P. P.; Misra, M. *Chem. Mater.* **2008**, *20*, 6784.
(15) Wang, Q.; Zhu, K.; Neale, N. R.; Frank, A. J. *Nano Lett.* **2009**, *9*, 806.
(16) Mohapatra, S. K.; Banerjee, S.; Misra, M. *Nanotechnology* **2008**, 19.
(17) Chen, S. G.; Paulose, M.; Ruan, C.; Mor, G. K.; Varghese, O. K.; Kouzoudis, D.; Grimes, C. A. *J. Photochem. Photobiol., A* **2006**, *177*, 177.
(18) Seabold, J. A.; Shankar, K.; Wilke, R. H. T.; Paulose, M.; Varghese, O. K.; Grimes, C. A.; Choi, K. S. *Chem. Mater.* **2008**, *20*, 5266.
(19) Macak, J. M.; Gong, B. G.; Hueppe, M.; Schmuki, P. *Adv. Mater.* **2007**, *19*, 3027.
(20) Macak, J. M.; Zollfrank, C.; Rodriguez, B. J.; Tsuchiya, H.; Alexe, M.; Creil, P.; Schmuki, P. *Adv. Mater.* **2009**, *21*, 3121.
(21) Li, D.; Chien, C.-J.; Deora, S.; Chang, P.; Lu, J. G. *Nanotechnology* **2010**, submitted.

Published on Web 09/21/2010

Herein, the versatile method is carried out to fill the nanotubes with various metals. Interestingly, high-yield metallic tubes are observed in ATO tubes arising from the conductive nature of TiO_2. Subsequently, the reductive doping is further applied in constructing dye-sensitized solar cells (DSSCs). The increased conductivity of nanotube bottoms reduces series resistance (R_s) in the DSSCs, leading to enhanced performance.

2. Experimental Section

Self-organized ATO nanotube films are prepared by a two-step anodization method on titanium foil (0.3 mm thickness, 99.5% purity). The first-step anodization is performed under 60 V for 4 h in ethylene glycol solution containing 0.3 wt % NH_4F and 2 wt % H_2O. The ATO film can be easily detached from the titanium substrate by employing the adhesive tape. The self-ordered concaves on the bare titanium substrate are then exposed. The second-step anodization is carried out in the same electrolyte to create a highly ordered tubular structure. The as-anodized TiO_2 nanotubes are recrystallized in ambient air under 580 °C for 6 h with the heating/cooling rates at 2 °C/min.

The as-prepared films are reductively doped in a conventional three-electrode electrochemical system, where the TiO_2 nanotubes serve as the working electrode, Ag/AgCl saturated in 3 M NaCl serves as the reference electrode, and a platinum wire is used as the counter electrode. The doping process is achieved by applying cyclic voltammetry for 10 cycles in 1 M NH_4Cl aqueous solution at a scan rate of 100 mV/s. Cu and Ni metals are then electrodeposited into ATO nanotubes (> 10 μm in length) via AC electrodeposition (1 Hz, 0.1 V amplitude vs Ag/AgCl).

The doped ATO films (~20 μm thickness) are also adopted in the DSSC assembly. In brief, ATO films (after three cycles of reductive doping) are first immersed in 0.2 M $TiCl_4$ solution for 2 h at room temperature, followed by an annealing treatment at 450 °C for 30 min. Dye loading is then performed by dipping the film into a 0.3 mM N719 dye (Solaronix) in *t*-butanol/acetonitrile solution (1:1 volume ratio) for 24 h. A Parafilm tape (127 μm) is used as a spacer layer between the ATO film and a counter electrode (ITO/glass) with a platinum (2 nm) coating. The electrolyte containing 0.5 M LiI, 0.05 M I_2, 0.5 M *tert*-butylpyridine in acetonitrile and valeronitrile (1:1 volume ratio) is then injected into the assembled DSSCs.

3. Results and Discussion

After the first-step anodization, the oxide film possesses self-organized nanotube arrays at the bottom,[21] while the top shows a disordered porous surface, as imaged in Figure 1a. Figures 1b and 1c represent the cross section and top views of ATO film, following the second-step anodization. The intertube distance is ~150 nm, about the same as the outer diameter of the tube. Figure 1d shows the bottom view of ATO membrane, where the tube bottom layer is partially removed.

Note that the tube wall thickness at the top layer is much thinner than that of the bottom layer, because of the longer duration of chemical dissolution. The barrier layer thickness at the bottom is estimated to be 60 nm. The presence of trace amounts of elemental fluorine is observed from the energy-dispersive X-ray spectroscopy (EDX) analysis (see inset of Figure 1d), indicating that the migration of F^- ions is driven by the electric field.

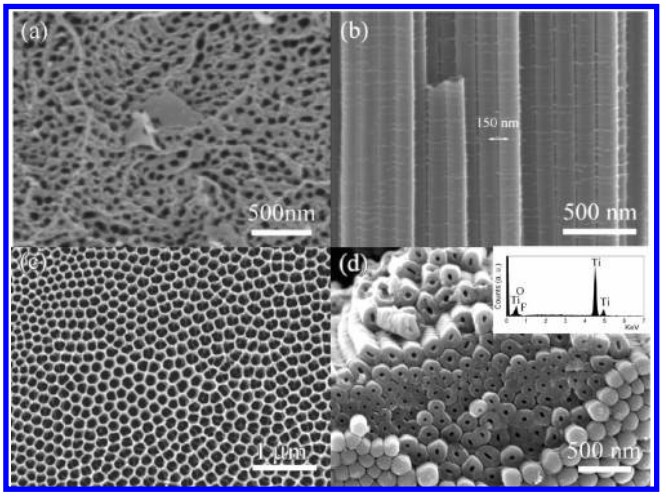

Figure 1. (a) SEM image of ATO film top surface after first-step anodization. (b) Side, (c) top, and (d) bottom views of ATO nanotube film after second-step anodization. Inset of panel (d) shows the EDX spectrum of nanotubes taken from bottom, indicating the existence of elemental fluorine.

Figure 2a plots the curve of current density, with respect to time ($J-t$) in the initial anodization state, which is similar to the anodizing behavior of porous aluminum oxide. As a result, it is reasonable to expect that the steady-state growth of nanotubes starts from stage "A", as marked in Figure 2a.[10,22] Considerable current fluctuation could arise from the suppressed heat transfer around the electrodes in an ethylene glycol solution. To crystallize the as-synthesized amorphous structure, an annealing process is conducted. The previous result shows that anatase phase and a trace amount of thermally grown rutile structure dominate after the annealing treatment.[9] A conductive AFM tip coated with Ti/Pt is applied to perform resistance measurement (as illustrated in the inset of Figure 2b) on the prepared nanotube arrays with a channel length of ~300 nm. Figure 2b depicts the current−voltage ($I-V$) curve, which shows a rectifying behavior of the Schottky barrier, because of the contact potential barrier between platinum (ϕ = 5.2) and TiO_2 (ϕ = 3.9 eV).[23] The maximum resistance obtained from the linear region of the $I-V$ curve is estimated to be ~2.27 MΩ. Although the resistivity cannot be accurately derived from the measurement, because of the existence of a contact barrier, the enhancement in conductance promotes the electrodeposition onto the nanotube side wall surface.

The reductive doping method has proven to be an efficient method to facilitate conductive TiO_2 films.[19,21,24−26] In the doping process, the Ti^{4+} ions at the nanotube barrier layer can be reduced to Ti^{3+} ions ($Ti^{4+}O_2 + e^- + H^+ \rightarrow Ti^{3+}(O)(OH)$). The Ti^{3+} dopant as a donor center results in a more conductive barrier layer, compared to the intact sidewall, which allows the "bottom-up" filling in the later electrodeposition process. A high-quality core−shell Cu_2O

(22) Thompson, G. E. *Thin Solid Films* **1997**, *297*, 192.
(23) Konenkamp, R.; Rieck, I. *Mater. Sci. Eng. B* **2000**, *69*, 519.
(24) Lyon, L. A.; Hupp, J. T. *J. Phys. Chem. B* **1999**, *103*, 4623.
(25) Pelouchova, H.; Janda, P.; Weber, J.; Kavan, L. *J. Electroanal. Chem.* **2004**, *566*, 73.
(26) Sakai, N.; Fujishima, A.; Watanabe, T.; Hashimoto, K. *J. Electrochem. Soc.* **2001**, *148*, E395.

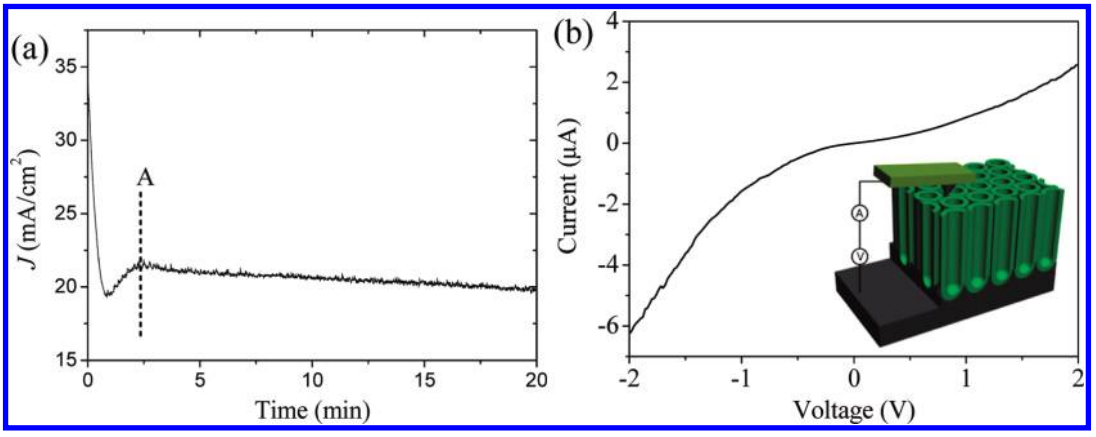

Figure 2. (a) Current density versus time ($J-t$) transient during anodization with an applied voltage of 60 V. (b) Current−voltage ($I-V$) curve measured by contacting an individual nanotube. Inset in panel (b) is a schematic depicting the use of a conductive AFM probe to address and measure TiO_2 nanotube arrays, where the titanium substrate serves as the bottom electrode.

nanowire/TiO_2 nanotube heterojunction along the radial direction has been demonstrated in our recent work, demonstrating enhanced solar cell performance.[21] The 1D system in a 3D matrix provides an ideal geometry with increased junction area, as well as a direct electron pathway with enhanced charge separation.[27−29]

Electrodeposition following the reductive doping is further confirmed here as a versatile approach in constructing 3D heterojunctions. For instance, copper metal is filled into the nanotubes (length of >10 μm) by AC electrodeposition (1 Hz, 0.1 V amplitude vs Ag/AgCl) in the electrolyte containing 300 g/L $CuSO_4$ and 45 g/L H_3BO_3. To evaluate the bottom doping effect on metal electrodeposition, the ATO with both doped and undoped areas is exposed to an electrolyte for deposition. A uniform copper film is formed in the doped area, whereas copper can be seldom observed in the upper side, as shown in Figure 3a. This suggests that the reductive doping treatment favors the uniform filling in the nanotube matrix. Expectedly, the as-deposited copper with a tubular structure has an outer diameter that is consistent with the inner diameter of the ATO tubes (see Figure 3b). An almost 100% filling rate is observed from the top view, as shown in the inset of Figure 3b.

Similar tubular structures have been observed in template-based electrodeposition in porous anodic aluminum oxide (AAO).[30,31] In contrast to the insulating AAO, the conducting nature of crystallized TiO_2 provides a continuous pathway for the metal electroplating onto the inner sidewalls of the tubes. In addition, the nanoscale channels with a high aspect ratio inhibit ionic diffusion and promote the formation of the tube-in-tube structure.[31]

Nickel nanotubes are also routinely formed in Ni^{2+}-based solution (120 g/L $NiSO_4 \cdot 6H_2O$ and 45 g/L H_3BO_3) by AC electrodeposition (1 Hz, 0.1 V vs Ag/AgCl), as shown in Figure 3c. X-ray diffraction (XRD) patterns of nanotube arrays of embedded ATO nanotubes are presented in Figure 3d, which can be indexed to face-centered cubic copper (JCPDS Card No. 4-0836) and nickel (JCPDS Card No. 4-0850), respectively. The unlabeled peaks arise from anatase (JCPDS Card No. 21-1272), rutile (JCPDS Card No. 21-1276) TiO_2, and the titanium substrate (JCPDS Card No. 44-1294).

Besides serving as a nanotemplate for constructing 3D core−shell structures, the modified ATO nanotubes can also be used to optimize the solar cell performances of TiO_2-based DSSCs. TiO_2 photoanodes are well-known to be the best candidate in DSSCs.[1,2] The electron diffusion length, depending on the diffusion coefficient and lifetime of the photon-generated electrons, is in the range of 10−30 μm for nanoparticle film.[32] In contrast, the diffusion length is greatly increased, on the order of 100 μm in ATO nanotube, benefiting from the efficient charge separation and transfer along the 1D nanotubes.[33] Thereby, film with a longer nanotube length could be adopted in the nanotube system with extra surface area for dye-loading purposes. Inspired by the recently developed technique on ATO nanotube synthesis, researchers have intensively studied the nanotubes-based DSSCs.[5,34−38] However, the energy conversion efficiency is still unsatisfactory. One possible reason originates from the relatively high resistivity of the TiO_2 nanotube matrix.

(27) Czaban, J. A.; Thompson, D. A.; LaPierre, R. R. *Nano Lett*. **2009**, *9*, 148.
(28) Fan, Z.; Razavi, H.; Do, J.-w.; Moriwaki, A.; Ergen, O.; Chueh, Y.-L.; Leu, P. W.; Ho, J. C.; Takahashi, T.; Reichertz, L. A.; Neale1, Steven; Yu, Kyoungsik; Wu, M.; Ager, J. W.; Javey, A. *Nat. Mater*. **2009**, *8*, 648.
(29) Taberna, P. L.; Mitra, S.; Poizot, P.; Simon, P.; Tarascon, J.-M. *Nat. Mater*. **2006**, *5*, 567.
(30) Lee, W.; Scholz, R.; Niesch, K.; Gösele, U. *Angew. Chem., Int. Ed*. **2005**, *44*, 6050.
(31) Li, D.; Thompson, R. S.; Bergmann, G.; Lu, J. G. *Adv. Mater*. **2008**, *20*, 4575.
(32) Fisher, A. C.; Peter, L. M.; Ponomarev, E. A.; Walker, A. B.; Wijayanta, K. G. U. *J. Phys. Chem. B* **2000**, *104*, 949.
(33) Jennings, J. R.; Ghicov, A.; Peter, L. M.; Schmuki, P.; Walker, A. B. *J. Am. Chem. Soc*. **2008**, *130*, 13364.
(34) Shankar, K.; Bandara, J.; Paulose, M.; Wietasch, H.; Varghese, O. K.; Mor, G. K.; LaTempa, T. J.; Thelakkat, M.; Grimes, C. A. *Nano Lett*. **2008**, *8*, 1654.
(35) Paulose, M.; Shankar, K.; Varghese, O. K.; Mor, G. K.; Hardin, B.; Grimes, C. A. *Nanotechnology* **2006**, *17*, 1446.
(36) Kuang, D.; Brillet, J.; Chen, P.; Takata, M.; Uchida, S.; Miura, H.; Sumioka, K.; Zakeeruddin, S. M.; Grätzel, M. *ACS Nano* **2008**, *2*, 1113.
(37) Paulose, M.; Shankar, K.; Varghese, O. K.; Mor, G. K.; Grimes, C. A. *J. Phys. D: Appl. Phys*. **2006**, *39*, 2498.
(38) Liu, Y.; Wang, H.; Li, M.; Hong, R. J.; Ye, Q. H.; Zheng, J. M.; Shen, H. *Appl. Phys. Lett*. **2009**, *95*, 233505.

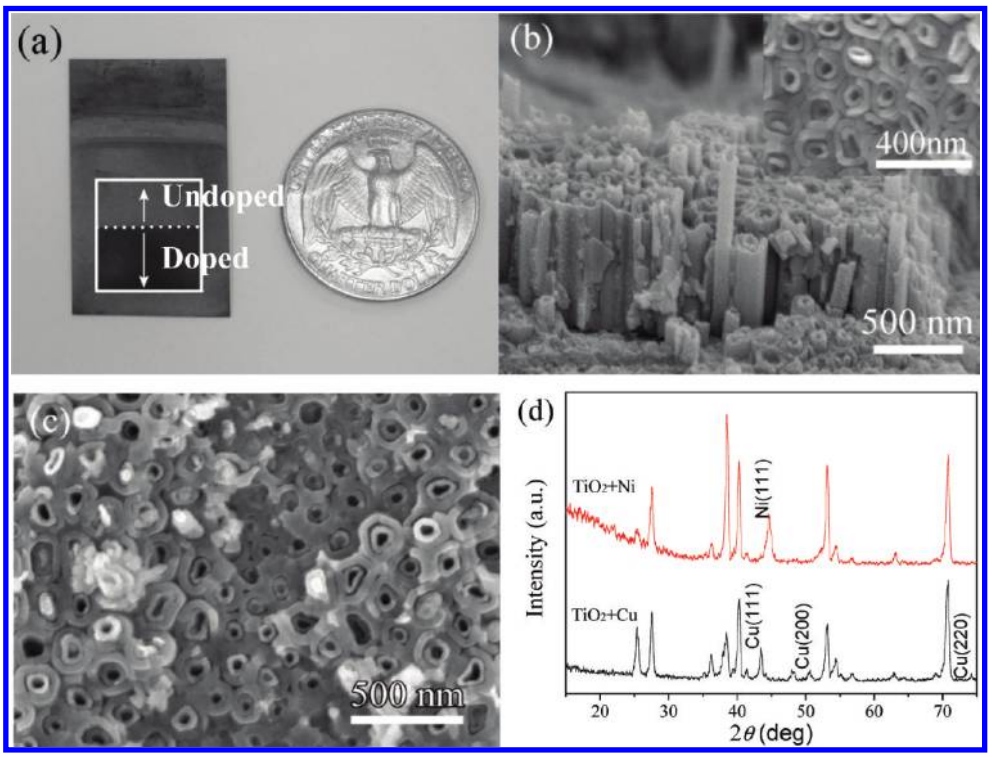

Figure 3. (a) Photograph of a TiO_2 nanotube template with and without copper electrodeposition. The lower side (after NH_4Cl treatment) is covered by a uniform copper film. (b) Oblique and top (inset) views of copper nanotubes embedded in ATO nanotube arrays. (c) Scanning electron microscopy (SEM) image of nickel nanotubes embedded in ATO nanotube arrays. (d) X-ray diffraction (XRD) patterns of copper and nickel nanotubes embedded in ATO nanotubes.

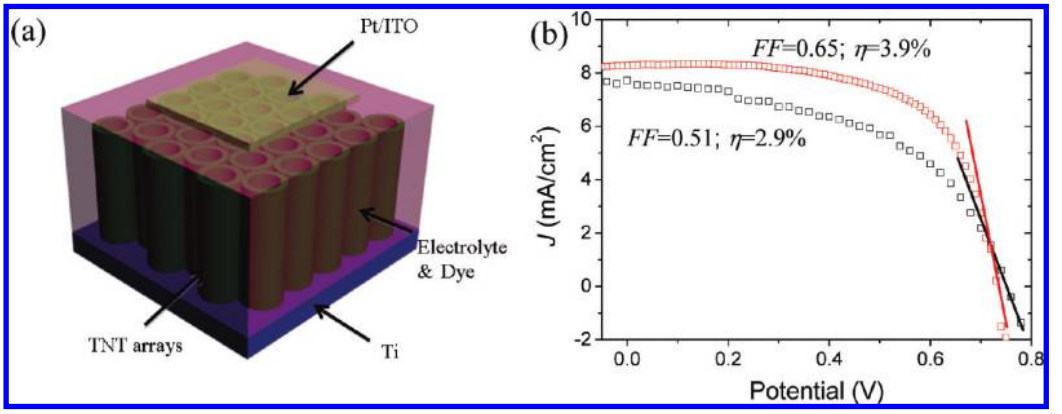

Figure 4. (a) Schematic diagram of ATO nanotubes-based DSSC. (b) $J-V$ characteristics of DSSCs with (red) and without (black) reductive doping treatment. The series resistances can be roughly estimated from the slopes at the open-circuit voltage (V_{oc}).

Especially, the high resistance in the tubes bottom renders a higher R_s, which leads to the suppressed fill factor (FF) and short-circuit current (I_{SC}).

Figure 4a illustrates the architecture of nanotube-based DSSCs. To improve the conductance of the TiO_2 nanotube matrix, the doping method mentioned above is applied on the ATO films. For comparison, DSSCs without a bottom treatment are also fabricated. The thickness of all employed nanotube films is ~20 μm. The photocurrent density−voltage ($J-V$) characteristics of the cells are measured under simulated AM 1.5 illumination (100 mW/cm^2), provided by a 300 W solar simulator (Newport).

The $J-V$ characteristics of DSSCs with and without bottom doping treatment are plotted in Figure 4b. Without doping treatment, the ATO-based DSSCs yield an overall power conversion efficiency (η) of 2.9% with a short-circuit current density (J_{sc}) of 7.72 mA/cm^2, open-circuit voltage (V_{oc}) of 0.74 V, and fill factor (FF) of 0.51. By employing the reductive doped ATO, the DSSC shows an enhanced photo conversion efficiency ($\eta \approx 3.9\%$) with increased J_{sc} and FF values (8.28 mA/cm^2 and 0.65, respectively). The open-circuit voltage remains the same (V_{oc} = 0.74 V, given by the energy level difference between the Fermi level of TiO_2 and the redox potential of the electrolyte). In an ideal cell, the total current I can be expressed by the photocurrent (I_{ph}) and the diode current (I_d):

$$I = I_{ph} - I_d = I_{ph} - I_0\left[\exp\left(\frac{V+IRs}{\eta kT}\right) - 1\right] - \frac{V+IR_s}{R_{sh}} \quad (1)$$

where I_0 is the diode reverse saturation current, η the ideality factor, V the output voltage, and R_{sh} the shunt resistance. R_{sh}, approximated from the slope of the reverse $J-V$ sweep at J_{sc}, is on the order of 1×10^3 Ω cm^2 for both devices. R_s shows a significant improvement from 20.5 Ω cm^2 to 10.2 Ω cm^2, that can be estimated from the slopes of the $J-V$ curves at V_{oc}.

Further improvements on the ATO photoanodes are under investigation for better solar cell performance. First, to balance electron transport (shorter length) and dye loading (longer length), an optimal channel length must be determined. Second, front-side orthogonal illumination geometry can be applied to enhance the energy conversion efficiency.[5,37,38] The current method of back-side illumination inhibits the cell performance, because photons will be largely reflected by platinized indium tin oxide (ITO)/glass.

4. Conclusions

Highly ordered anodic titanium oxide (ATO) nanotubes with enhanced bottom conductivity are achieved by reductive doping in electrochemical cells. Three-dimensional (3D) tube-in-tube structures are achieved by simple electrochemical deposition, which holds far reaching potential applications in catalyst, battery, supercapacitor, etc. Moreover, the bottom-treated nanotubes, serving as photoanodes, are assembled into dye-sensitized solar cells. As a benefit from the reduction of series resistance, the as-fabricated solar cells demonstrate improved performance with enhanced fill factor (FF) and short-circuit current density (J_{SC}).

Acknowledgment. The authors thank Mr. Akshay Kumar and Mr. Zuwei Liu for their helpful discussions and technical assistance. The work is supported by DOE EFRC program.

Note Added after ASAP Publication. There were minor text errors throughout the paper in the version published ASAP September 21, 2010; the corrected version was published ASAP September 24, 2010.